Science
AAAS

An Exhumation History of Continents over Billion-Year Time Scales
Terrence J. Blackburn, *et al.*
Science **335**, 73 (2012);
DOI: 10.1126/science.1213496

Science (print ISSN 0036-8075; online ISSN 1095-9203) is published weekly, except the last week in December, by the American Association for the Advancement of Science, 1200 New York Avenue NW, Washington, DC 20005.

than in the *c* direction, thus resulting in the thin hexagonal-plate form due to the limited crystal growth via the layer-by-layer mechanism along the *c* direction (*29*).

The homogeneity of the two samples, ultrasmall (6- to 15-nm) and nanosized (50- to -70 nm) EMT crystals, is illustrated at two different magnifications in Fig. 4, A to D. The hexagonal morphology of both samples is evident. Moreover, their colloidal stability was examined by measuring the zeta potential values, which are equal to –45 mV. This negative charge leads to electrostatic stabilization of the hexagonal nanoparticles.

Why has EMT never been observed in organic-free synthesis solutions? The reason may be surprisingly simple. When the same synthesis solutions as described above were heated at the same temperature for extended times or at higher temperatures, the nanoscale EMT materials converted into the well-known FAU and SOD structures (fig. S2). We propose that under appropriate conditions the EMT is the first kinetic, metastable product in this synthesis field, followed by conversion into the more stable cubic FAU and more dense SOD structures. This hypothesis is strongly supported by several reports on EMT/FAU intergrowths (*9*–*14*). Indeed, we suggest that it may be possible to capture other important zeolite phases that occur as intergrowths by exploiting the very early stages of synthesis and thus avoiding the use of organic reagents that are commonly needed to stabilize the desired phases.

From an environmental perspective, the synthesis of EMT zeolite presented here is extremely attractive, as the nanocrystals can be easily synthesized at very high yield at near ambient temperature without using any organic templates, suggesting that scale-up of an energy-efficient synthesis would be easily feasible. These nanoscale EMT materials offer exciting opportunities for both fundamental study and potential industrial applications. The possible green mass production of EMT-type zeolite provides excellent opportunities for applications in catalysis, adsorption, and separations involving larger molecules and for designing thin films, membranes, or nanoscale devices.

References and Notes

1. M. E. Davis, *Nature* **417**, 813 (2002).
2. D. W. Breck, *Zeolites and Molecular Sieves System* (Wiley, New York, 1974).
3. J. Choi *et al.*, *Science* **325**, 590 (2009).
4. M. A. Snyder, M. Tsapatsis, *Angew. Chem. Int. Ed.* **46**, 7560 (2007).
5. Ch. Baerlocher, L. B. McCusker, D. H. Olson, in *Atlas of Zeolite Framework Types* (Elsevier, Amsterdam, Netherlands, ed. 6, 2007), p. 123.
6. D. E. W. Vaughan, in *Properties and Applications of Zeolites*, R. P. Townsend, Ed. (The Chemical Society, London, 1980), p. 294.
7. F. Dougnier, J. Patarin, J.-L. Guth, D. Anglerot, *Zeolites* **12**, 160 (1992).
8. S. Liu, L. Li, C. Li, X. Xiong, F.-S. Xiao, *J. Porous Mater.* **15**, 295 (2008).
9. A. Haas, D. A. Harding, J. R. D. Nee, *Microporous Mesoporous Mater.* **28**, 325 (1999).
10. M. G. Barrett, D. E. W. Vaughan, UK Patent GB 2,076,793 A (1981).
11. D. E. W. Vaughan, European Patent 0,351,461 (1989).
12. J. M. Newsam, M. M. J. Treacy, D. E. W. Vaughan, K. G. Strohmaier, W. J. Mortier, *Chem. Commun.* 493 (1989).
13. G. T. Kokotailo, J. Ciric, *Adv. Chem. Ser.* **101**, 109 (1971).
14. J. A. Martens, P. A. Jacobs, S. Cartlidge, *Zeolites* **9**, 423 (1989).
15. F. Dougnier, J. L. Guth, *Microporous Mater.* **6**, 79 (1996).
16. R. Wendelbo, M. Stöcker, H. Junggreen, H. B. Mostad, Norwegian Patent Application No. 964988 (2001).
17. R. Wendelbo, M. Stöcker, H. Junggreen, H. B. Mostad, D. E. Akporiaye, *Microporous Mesoporous Mater.* **28**, 361 (1999).
18. M. Matsukata, K. Kizu, M. Ogura, E. Kikuchi, *Cryst. Growth Des.* **1**, 509 (2001).
19. J. Sun, M. Sun, C. Nie, Q. Li, *J. Chem. Soc. Chem. Commun.* 2459 (1999).
20. Y. Luo, J. Sun, W. Zhao, J. Yao, Q. Li, *Chem. Mater.* **14**, 1906 (2002).
21. T. Chatelain, J. Patarin, M. Soulard, J. L. Guth, P. Shulz, *Zeolites* **15**, 90 (1995).
22. S. L. Burkett, M. E. Davis, *Microporous Mater.* **1**, 265 (1993).
23. S. Mintova, N. H. Olson, V. Valtchev, T. Bein, *Science* **283**, 958 (1999).
24. B.-Z. Zhan *et al.*, *Chem. Mater.* **14**, 3636 (2002).
25. S. Mintova, M. Reinelt, T. H. Metzger, J. Senker, T. Bein, *Chem. Commun.* **2003**, 326 (2003).
26. L. Tosheva, V. Valtchev, *Chem. Mater.* **17**, 2494 (2005).
27. J. L. Casci, *Microporous Mesoporous Mater.* **82**, 217 (2005).
28. A. Le Bail, *J. Non-Cryst. Solids* **183**, 39 (1995).
29. G. González, C. S. González, W. Stracke, R. Reichelt, L. García, *Microporus Mesoporus Mater.* **101**, 30 (2007).
30. D. Chateigner, in *Combined Analysis: Structure-Texture-Microstructure-Phase-Stresses-Reflectivity Determination by X-ray and Neutron Scattering* (Wiley, New York, 2010), p. 410.
31. L. Lutterotti, S. Matthies, H.-R. Wenk, in *MAUD (Material Analysis Using Diffraction): A User Friendly JAVA Program for Rietveld Texture Analysis and More*, in *Textures of Materials*, J. A. Szpunar, Ed. (National Research Council Canada Research Press, Ottawa, 2002), p. 1599.
32. N. C. Popa, *J. Appl. Cryst.* **31**, 176 (1998).

Acknowledgments: We thank S. Schmidt (LMU) for collecting the TEM data and SRIF-ANR-06-NANO-007-01 Region and FEDER of Down Normandy, NIM (Nano-Initiative-Munich), for financial support.

Supporting Online Material

www.sciencemag.org/cgi/content/full/science.1214798/DC1
SOM Text
Figs. S1 to S12
Tables S1 to S5

3 October 2011; accepted 11 November 2011
Published online 8 December 2011;
10.1126/science.1214798

An Exhumation History of Continents over Billion-Year Time Scales

Terrence J. Blackburn,[1]* Samuel A. Bowring,[1] J. Taylor Perron,[1] Kevin H. Mahan,[2] Francis O. Dudas,[1] Katherine R. Barnhart[2]

The continental lithosphere contains the oldest and most stable structures on Earth, where fragments of ancient material have eluded destruction by tectonic and surface processes operating over billions of years. Although present-day erosion of these remnants is slow, a record of how they have uplifted, eroded, and cooled over Earth's history can provide insight into the physical properties of the continents and the forces operating to exhume them over geologic time. We constructed a continuous record of ancient lithosphere cooling with the use of uranium-lead (U-Pb) thermochronology on volcanically exhumed lower crustal fragments. Combining these measurements with thermal and Pb-diffusion models constrains the range of possible erosion histories. Measured U-Pb data are consistent with extremely low erosion rates persisting over time scales approaching the age of the continents themselves.

The preservation of fragments of stable Archean continental lithosphere, or "cratons," over geologic time is intimately linked with the presence of a low-density mantle root that supports and protects the overlying crust (*1*). The long-term stability of these roots has been attributed to an apparent "isopycnic" balance between the negative thermal buoyancy from contraction during cooling and the positive chemical buoyancy from the depletion of the root's denser basaltic component during craton formation (*1*, *2*). Despite this stability, cratons must survive exposure to surface processes working to erode on durations lasting billions of years, a process that results in continued rock exhumation toward Earth's surface. Although present-day erosion within these stable regions is low, the assembly of continental masses through mountain-building processes (*3*) requires that these terranes experienced periods of rapid erosion after the construction of topographically high mountain belts. An erosional history recording the duration of this early rapid erosional phase and the timing and rate of transition to the slow erosion observed today will allow us to understand more about the composition and density of the lithosphere, its relationship with the underlying mantle, and the thermal, buoyant, and mechanical forces operating to exhume or bury the continents over the geologic history of Earth.

Because the exhumation or burial of Earth's surface has a direct effect on the rate of heat loss within the lithosphere, a continuous record

[1]Earth Atmospheric and Planetary Sciences, Massachusetts Institute of Technology, Cambridge, MA 02139, USA. [2]Department of Geological Sciences, University of Colorado, Boulder, CO 80309, USA.

*To whom correspondence should be addressed. E-mail: terrence@mit.edu

of lithosphere exhumation can be reconstructed through the use of a temperature-sensitive radiometric dating technique known as thermochronology. The combination of thermochronologic data with thermal models for heat transfer in the lithosphere can be used to measure the processes operating to cool or heat the lithosphere in the geologic past (*4*). Thermochronologic studies have typically used geochronologic systems sensitive to cooling at temperatures below 110°C. These techniques are most useful for the measurement of cooling attributable to deformation in the upper crust and erosion of topography (*5*). A thermochronologic system sensitive to cooling at higher temperatures and greater depths is insensitive to the "noise" associated with near-surface cooling and therefore provides a measure of the background rate of erosion or burial associated with the vertical motions of a craton. The U-Pb thermochronologic system is sensitive to cooling at temperatures of ~400° to 650°C, corresponding to lower crustal depths in cratonic regions of ~20 to 50 km (*6*). Here, we used this technique to reconstruct an ancient and long-lived thermal history of volcanically exhumed lower crustal fragments—samples that resided at depth for billions of years before recent volcanism transported them to the surface as xenoliths. A high-fidelity reconstruction of time-temperature paths for these samples is produced using the U-Pb system's dual decay scheme, where parent isotopes ^{238}U and ^{235}U decay at different rates to daughter isotopes ^{206}Pb and ^{207}Pb, respectively. Coupling this dual isotopic system with diffusion's length scale dependency, which causes different crystal sizes to retain Pb over different absolute time scales, results in a set of daughter isotopic compositions for a range of crystal sizes that is unique to the time-temperature history of the sample (*7*). The measured and modeled U-Pb results presented here explore a range of crystal grain sizes to exploit these advantages (*8*).

The thermal processes operating to cool or heat the deep lithosphere include conductive heat loss, heat input from the underlying mantle, heat production from the decay of heat-

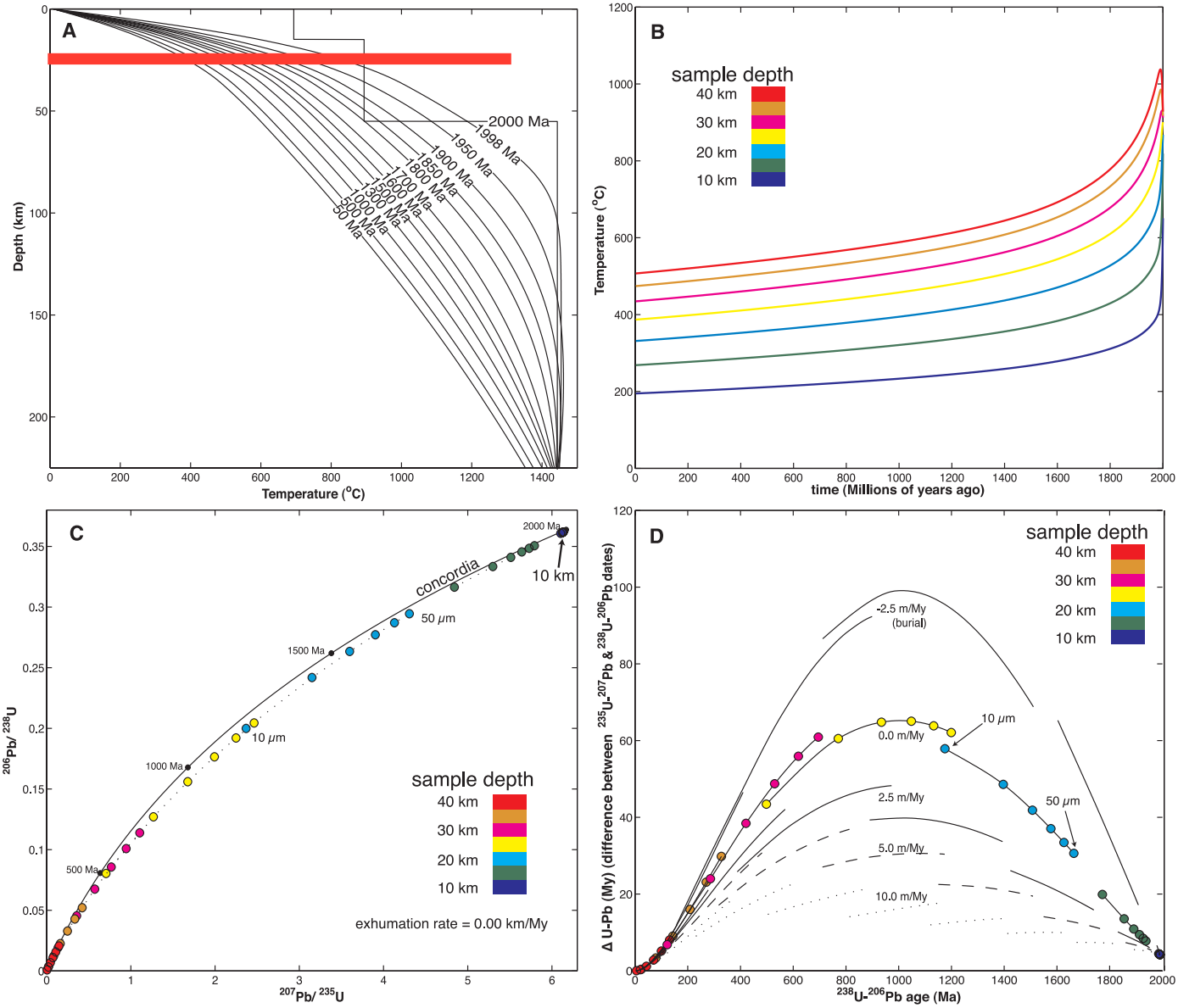

Fig. 1. (**A** and **B**) Thermal history for the lithosphere (A) used to produce time-temperature paths (B) for samples at middle to lower crustal depths. (**C** and **D**) Time-temperature paths are used to calculate modeled U-Pb thermochronologic data for each sample depth (colors) and over a range of grain sizes. The "concordia" curve in (C) represents the daughter-to-parent ratios of ^{235}U-^{207}Pb and ^{238}U-^{206}Pb for a U-Pb system that remains closed throughout Earth history. The shallowest samples cool quickly through the Pb partial retention zone (PRZ), yielding old ^{238}U-^{206}Pb dates that plot on concordia (C) or yield Δ U-Pb values close to zero (D). The deepest samples reside at temperatures that are too hot for Pb retention in rutile, and thus yield younger dates. The middle to lower crust spends a long time in the Pb-PRZ, resulting in discordance (C) and a large apparent offset between the two U-Pb systems (D). The magnitude of Δ U-Pb values (D) is correlated with lithosphere exhumation rate.

producing elements (HPEs), and cooling or insulation due to surface erosion or burial, respectively. The combined effects of these processes on the U and Pb isotopic evolution of a set of rutile crystals can be described with a simple thermal model (*8*). The modeled lithosphere thermal history begins with a steep geothermal gradient consistent with formation or reheating during mountain-building events, followed by cooling due to heat loss at the lithosphere surface (Fig. 1A). The time-temperature histories for crustal depths from the thermal model (Fig. 1B) are then used as the input to a model of Pb production and diffusion (*8*). Modeled U-Pb thermochronologic data correlate directly with sample depth (Fig. 1C). Shallow samples cool quickly through the 400° to 600°C rutile thermal window, yielding U-Pb dates that are consistent with the model start time, whereas the deepest samples never cool below the Pb closure for rutile, accumulate no radiogenic Pb, and yield U-Pb dates of 0 million years ago (Ma) (Fig. 1C). The faster-cooling, shallow samples yield dates that plot on the "concordia" curve (which represents the daughter-to-parent ratios of ^{235}U-^{207}Pb and ^{238}U-^{206}Pb for a U-Pb system that remains closed throughout Earth history), indicating agreement between the ^{238}U-^{206}Pb and ^{235}U-^{207}Pb systems and closed-system behavior. Samples at intermediate depths accumulate different amounts of radiogenic Pb, depending on depth, forming a curvilinear "discordant" array off the concordia curve that indicates partially open system behavior. Mineral grains that spend a long time in the Pb partial retention zone (PRZ)—a temperature range in which the diffusion and production of radiogenic daughters are at or near a balance—result in the partial retention of Pb with a range of isotopic compositions ($^{207}Pb/^{206}Pb$). A whole-crystal analysis yields an integrated measure of the internal Pb-diffusion profile, resulting in the apparent difference between the measured ^{235}U-^{207}Pb and ^{238}U-^{206}Pb dates (hereafter referred to as Δ U-Pb). Slower cooling, and thus longer durations in the PRZ, result in a Pb diffusion profile containing a wider range of $^{207}Pb/^{206}Pb$ compositions, and thus a greater Δ U-Pb age difference (Fig. 1D) (*7*). Because the vertical advection of lower crustal rocks toward Earth's surface increases the rate of cooling at depth, there is a strong correlation between the maximum Δ U-Pb value and net exhumation, where higher net exhumation rates yield lower Δ U-Pb values (Fig. 1D). The U-Pb system's sensitivity to cooling rate—and, in this thermal setting, to exhumation rate—is the key factor that allows constraints to be placed on the long-term evolution of continental surfaces.

Along the southwestern edge of the North American Craton within Montana, the Archean Medicine Hat Block and Wyoming Province collided at ~1800 Ma to form the Great Falls Tectonic Zone (GFTZ), a Proterozoic suture between the two terranes (*9*) (Fig. 2B, inset). Lower crustal xenoliths used in this study were collected from four ~50 Ma volcanic epicenters within each terrane. The volcanic entrainment of samples at 50 Ma is so rapid that U/Pb loss due to volcanic reheating is negligible (*7*). Lower crustal U-Pb thermochronologic data yield the "humped" topology of Δ U-Pb data predicted by

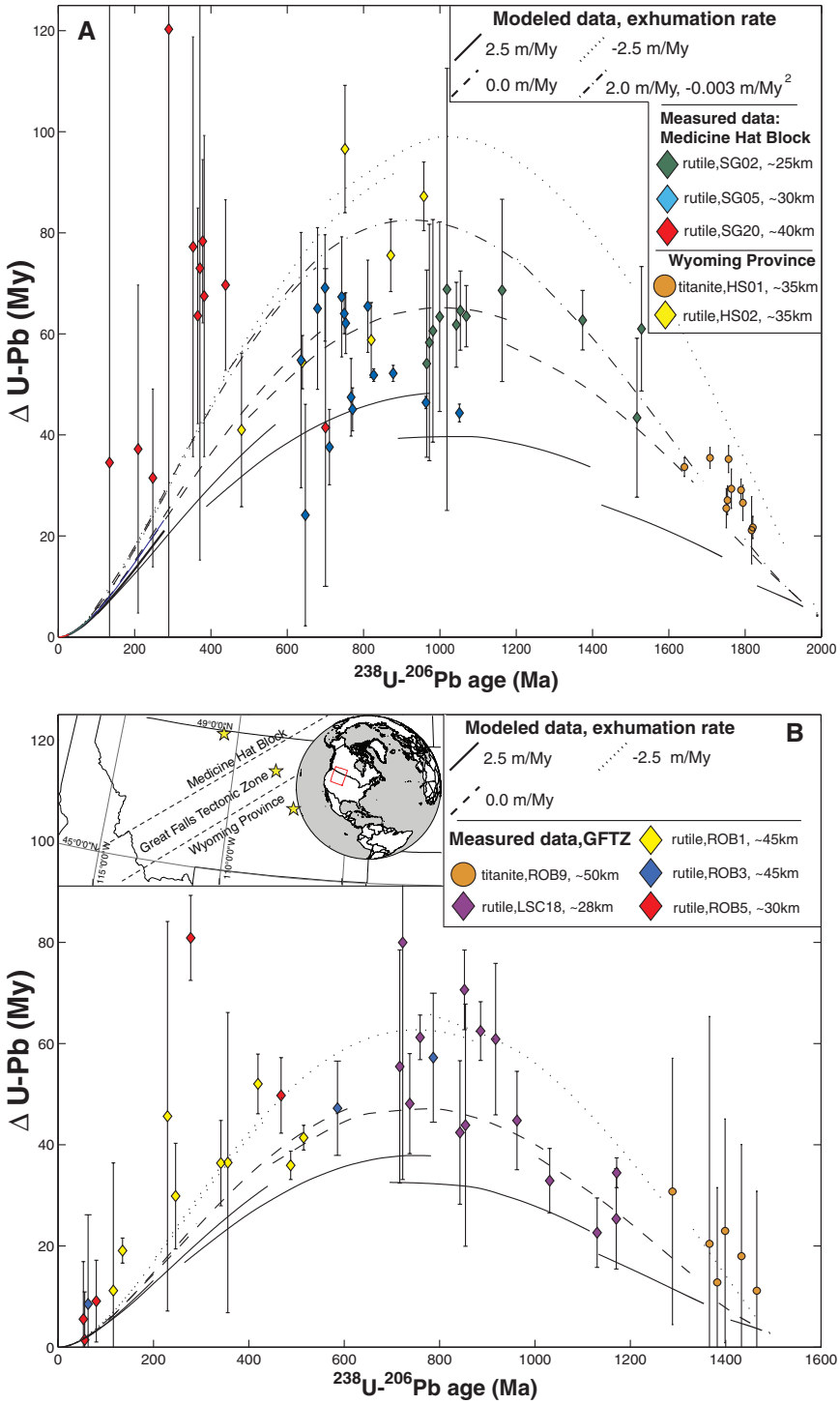

Fig. 2. Plots of Δ U-Pb versus time for measured and modeled lower crustal xenolith data from a northwest-southeast transect through Montana: **(A)** Archean Medicine Hat Block and Wyoming Province, **(B)** Proterozoic Great Falls Tectonic Zone (GFTZ). Sample numbers and geobarometrically determined depths are indicated. Faster-cooling, shallow samples yield older dates with a trend of increasing Δ U-Pb in time; deeper samples decrease with time, consistent with the results predicted by the thermal model (Fig. 1D). Uncertainties on individual analyses are shown at the 2σ level and are dominated by the uncertainty of the ^{235}U-^{207}Pb date. Dashed, dotted, and solid lines mark the forward-modeled U-Pb results with exhumation rates of −2.5 to 2.5 m/My. A dashed-dot line in (A) marks the data produced by an erosional history that decreased in time. The inset in (B) shows a simplified geologic terrane map of Montana; stars mark the xenolith sample location within each geologic terrane.

the thermal model (Fig. 1D), supporting the use of this model to infer lithosphere exhumation rate (Fig. 2). The onset of cooling in both regions is recorded by the higher-temperature titanite U-Pb thermochronometer. Within the Archean regions this occurs at ~2000 Ma, indicating the diffusive loss of an Archean cooling record during the younger reheating event (Fig. 2A). Within the Proterozoic GFTZ, the onset of cooling in the region does not occur until ~300 million years (My) after the formation of the inferred mountain belt—a delay in cooling that is consistent with rapid erosion rates between 1800 and 1500 Ma (Fig. 2B). The subsequent long-term cooling history in each terrane is recorded by the lower-temperature rutile thermochronometer, where analyses from xenoliths of different depths provide a continuous and overlapping cooling record lasting more than ~1500 My (Fig. 2). Thermobarometrically determined xenolith depths (*7*, *10*) correlate with the timing of cooling, with the shallowest samples cooling first and deeper samples cooling at progressively younger times (Fig. 2). Assuming an intermediate lithosphere thickness of 225 km (*11*–*13*) and the recommended HPE concentrations from compiled data sets (*14*, *15*), forward-modeled rutile data for a range of exhumation rates from –2.5 to 2.5 m/My (where a negative exhumation rate corresponds to burial) bracket the measured data (*8*) (Fig. 2). Secular variations in exhumation rate control the symmetry of the curves of Δ U-Pb versus time. For example, decreasing the exhumation rate over time skews the peak to the left, yielding modeled data that are also consistent with the measured results, yet their average exhumation rates are bracketed by those that assume constant exhumation (Fig. 2A).

Although the long-term exhumation rates reported here (–2.5 to 2.5 m/My) are in good agreement with shorter-duration observations of some of the slowest-eroding surfaces on Earth (*16*), they are far slower than what is observed for the majority of continental surfaces (50 to 500 m/My) (*16*). This disparity can be attributed to the difference in the time scales of observation and secular variations in exhumation. The exhumation rates presented here are long-term integrated estimates and do not preclude the occurrence of brief periods of faster exhumation associated with tectonic (*16*) or climatic forces (*17*) operating over intervals much shorter than the observational time scale for this technique. Once a continental mass is laterally isolated from active plate boundaries and vertically supported by a thickened mantle root, the long-term uplift of a mountain belt is more likely dominated by the relative densities of the lithosphere and mantle (isostasy) (*18*) with a potentially transient and smaller contribution to uplift or burial imposed by density and thermal anomalies in the underlying convecting mantle (dynamic topography) (*19*).

The U-Pb system's sensitivity to the magnitude and time variability of exhumation rate can be used to set limits on the timing and duration of events that exhumed or buried the surfaces of continents in the deep geologic past. First, we can gauge the duration of rapid erosional unroofing after mountain building from the difference between collision age and onset of cooling. Within the GFTZ (Fig. 2B), the 300-My difference between the onset of cooling and the mountain-building event establishes a maximum interval over which isostatically driven uplift can persist at the rates observed in young and topographically high mountain belts (50 to 100 m/My) (*18*). Second, we can rule out erosional histories that include periods of exhumation or burial faster than a given rate or longer than a given time interval (with a trade-off between duration and rate). For example, we can dismiss histories for the GFTZ with exhumation or burial lasting longer than 50 My at rates that exceed ±50 m/My. More subtle transient deformation mechanisms such as dynamic topography, with a characteristic amplitude less than 1 km over a distance of 1000 km or more, will be undetected on the short time scales (tens to hundreds of millions of years) and modest exhumation/burial rates (10 to 100 m/My) at which this process operates (*19*). Despite the possibility of brief erosional or burial events of moderate magnitude, the data presented here require an overall cratonic history dominated by vertical motion rates near zero. This indicates that the isostatic balance observed in the present-day continents has been largely maintained over geologic time, extending back at least to the onset of cooling within each terrane. Since this stability was first attained, the craton has experienced a balance between erosion and burial, with a corollary balance between the lithosphere's internal buoyancy forces (*1*, *2*) and near-zero isostatic uplift, further indicating a minimal change in the relative densities of the lithosphere and mantle over intervals lasting billions of years.

References and Notes

1. T. H. Jordan, *J. Petrol.* (special lithosphere issue), 11 (1988).
2. A. M. Forte, H. K. Perry, *Science* **290**, 1940 (2000).
3. P. F. Hoffman, *Annu. Rev. Earth Planet. Sci.* **16**, 543 (1988).
4. T. A. Ehlers, K. A. Farley, *Earth Planet. Sci. Lett.* **206**, 1 (2003).
5. J. Braun, *Earth Planet. Sci. Lett.* **200**, 331 (2002).
6. M. D. Schmitz, S. A. Bowring, *Contrib. Mineral. Petrol.* **144**, 592 (2003).
7. T. Blackburn, S. Bowring, B. Schoene, K. Mahan, F. Dudas, *Contrib. Mineral. Petrol.* **162**, 479 (2011).
8. See supporting material on *Science* Online.
9. P. A. Mueller, A. L. Heatherington, D. M. Kelly, J. L. Wooden, D. W. Mogk, *Geology* **30**, 127 (2002).
10. K. Barnhart, thesis, University of Colorado, Boulder (2011).
11. H. Yuan, B. Romanowicz, *Nature* **466**, 1063 (2010).
12. B. C. Hearn Jr., *Lithos* **77**, 473 (2004).
13. S. Burdick *et al.*, *Seismol. Res. Lett.* **79**, 384 (2008).
14. R. L. Rudnick, S. Gao, D. H. Heinrich, K. T. Karl, in *Treatise on Geochemistry*, R. L. Rudnick, Ed. (Pergamon, Oxford, 2003), pp. 1–64.
15. R. L. Rudnick, W. F. McDonough, R. J. O'Connell, *Chem. Geol.* **145**, 395 (1998).
16. E. W. Portenga, P. R. Bierman, *GSA Today* **21**, 4 (2011).
17. P. W. Reiners, T. A. Ehlers, S. G. Mitchell, D. R. Montgomery, *Nature* **426**, 645 (2003).
18. K. M. Fischer, *Nature* **417**, 933 (2002).
19. J. Braun, *Nat. Geosci.* **3**, 825 (2010).

Acknowledgments: We thank B. Hager, K. Burke, S. Hemming, and three anonymous referees for their constructive comments, and C. Hearn for contributions in sample collection. Supported by EarthScope grants EAR-0746205 (S.A.B.) and EAR-0746246 (K.H.M.). Previously unpublished U-Pb data are tabulated in table S1.

Supporting Online Material

www.sciencemag.org/cgi/content/full/335/6064/73/DC1
Materials and Methods
SOM Text
Figs. S1 to S3
Tables S1 and S2
References (*20*–*28*)

2 September 2011; accepted 28 November 2011
10.1126/science.1213496

Multiyear Prediction of Monthly Mean Atlantic Meridional Overturning Circulation at 26.5°N

Daniela Matei,[1]* Johanna Baehr,[2] Johann H. Jungclaus,[1] Helmuth Haak,[1] Wolfgang A. Müller,[1] Jochem Marotzke[1]*

Attempts to predict changes in Atlantic Meridional Overturning Circulation (AMOC) have yielded little success to date. Here, we demonstrate predictability for monthly mean AMOC strength at 26.5°N for up to 4 years in advance. This AMOC predictive skill arises predominantly from the basin-wide upper-mid-ocean geostrophic transport, which in turn can be predicted because we have skill in predicting the upper-ocean zonal density difference. Ensemble forecasts initialized between January 2008 and January 2011 indicate a stable AMOC at 26.5°N until at least 2014, despite a brief wind-induced weakening in 2010. Because AMOC influences many aspects of climate, our results establish AMOC as an important potential carrier of climate predictability.

Variations in Atlantic Meridional Overturning Circulation (AMOC) can substantially affect northward ocean heat transport and therefore European and North Atlantic climate (*1*–*3*). Through its influence on sea surface temperature (SST), AMOC is further-